Post-mortem analyses of gap facing surfaces of tungsten tiles of T-10 ring limiter

A. Pisarev[a], I. Arkhipov[b], Ya. Babich[a], M. Berdnikova[a], Yu. Gasparyan[a], K. Gutorov[a,c],
S. Grashin[d], V. Efimov[a], M. Isaenkova[a], S. Krat[a], O. Krymskaya[a], V. Kurnaev[a], T. Stepanova[a],
E. Vovchenko[a], I. Vizgalov[a], and M. Zibrov[e]

[a] National Research Nuclear University MEPhI, Moscow, Russia
[b] Frumkin Institute of Physical Chemistry and Eletrochemistry RAS, Moscow, Russia
[c] Troitsk Institute for Innovation and Fusion Research, Troitsk, Russia
[d] Russian Research Center "Kurchatov Institute", Moscow, Russia
[e] Max Planck Institute for Plasma Physics, 85748 Garching, Germany

aapisarev@mephi.ru

Abstract

Surfaces facing the gap between W tiles of the ring limiter of tokamak T-10 were analyzed after T-10 decommissioning using LIBS, SEM/EDA, XRD, TDS, and NRA techniques. Gaps with the width of 5 mm and 0.1 mm were nearly completely covered to their full depths of 22 and 15 mm, respectively, by a deposited film. The film was formed mainly by deposition of lithium that came from Li limiter and transformed in air to Li_2CO_3 and Li_2O. Carbon was deposited from volatile hydrocarbons sputtered from the tokamak walls. Besides, carbon appeared due to chemical reaction with lithium in air. Chemical interactions of W with C, O, and Li led to formation W_2C, WC, WO_2, and Li_2WO_4. Carbides formed in W over the entire surface to the full depth of the gaps. Trapping of deuterium and helium in tiles was demonstrated. Possible influence of auto-oscillating discharges on ionization and ion trapping of C,D, and He in gaps is discussed.

1. Introduction

Consequences of plasma surface interactions are usually analyzed on plasma facing surfaces. Gaps and remote areas are, nevertheless, subjected to indirect plasma impact. The most often observed effect is deposition of films due to transport of particles, which are sputtered from plasma facing surfaces. Carbon deposits were observed in many large and small-sized tokamaks either working with graphite plasma-facing components (PFC) or having graphite PFC in previous campaigns [1-21]. Deposits in gaps and remote areas were observed, for example, in TEXTOR [1, 14, 22], DIIID [2], JET [3, 7, 9, 12, 20, 21], JT-60U [8], TFTR [9], KSTAR [11], Tore Supra [13, 15], Alcator [17], and RFX [6]. The effect was interpreted as co-deposition of carbon with hydrogen and deposition of volatile hydrocarbons formed due to chemical sputtering of carbon [18, 19]. The concentration of carbon in gaps was usually found to decrease within a few millimeters from the gap entrance towards its bottom. Nevertheless, surprisingly high concentration of carbon at the very bottom of castellated structures installed in TEXTOR was found in [23].

Deep penetration of carbon in gaps was observed also in [24, 25] in simulation experiments with gaps subjected to the beam-plasma discharge. Deposition of carbon films was detected through the entire depth of the gaps including those that were as narrow as 0.1 mm. The effect was explained by auto-oscillating discharges formed on surfaces of the plates, which were analyzed in [26].

This paper is devoted to analysis of gap facing surfaces of two W tiles of the ring limiter of tokamak T-10, which form a gap, where heavy deposits were observed on its entire surface. Analyses were performed using several techniques, such as laser induced breakdown spectroscopy (LIBS), scanning electron microscopy (SEM), energy dispersive analyses (EDA), X-ray diffraction

(XRD), thermal desorption spectrometry (TDS), and nuclear reaction analyses (NRA). Description of the T-10 operation with the W limiter was given in [27].

2. Tiles for investigation

The ring limiter of T-10 (figure 1) was made as a stainless steel (SS) ring holder oriented perpendicular to the toroidal axis and W tiles bolted to the holder from the electron and ion sides. The two tiles formed a gap 5 mm in width and 22 mm in depth. All in all, there were 32 tiles on the electron side and 32 tiles on the ion side. The tiles were $67\times37\times10$ mm in dimensions and were cut from a rolled sheet made of powder sintered tungsten with a typical grain size of ≈ 30 μm produced by "Polema" (Tula, Russia) using the same technology as that proposed for production of divertor tiles for ITER. Rolled material had anisotropy of its properties, and this led to anisotropy of changes after plasma impact but did not influence film deposition. The density of material was 19.21 g/cm^3, and it is less than the table value 19.25 g/cm^3, which is indicative of porosity, observed in tiles by SEM.
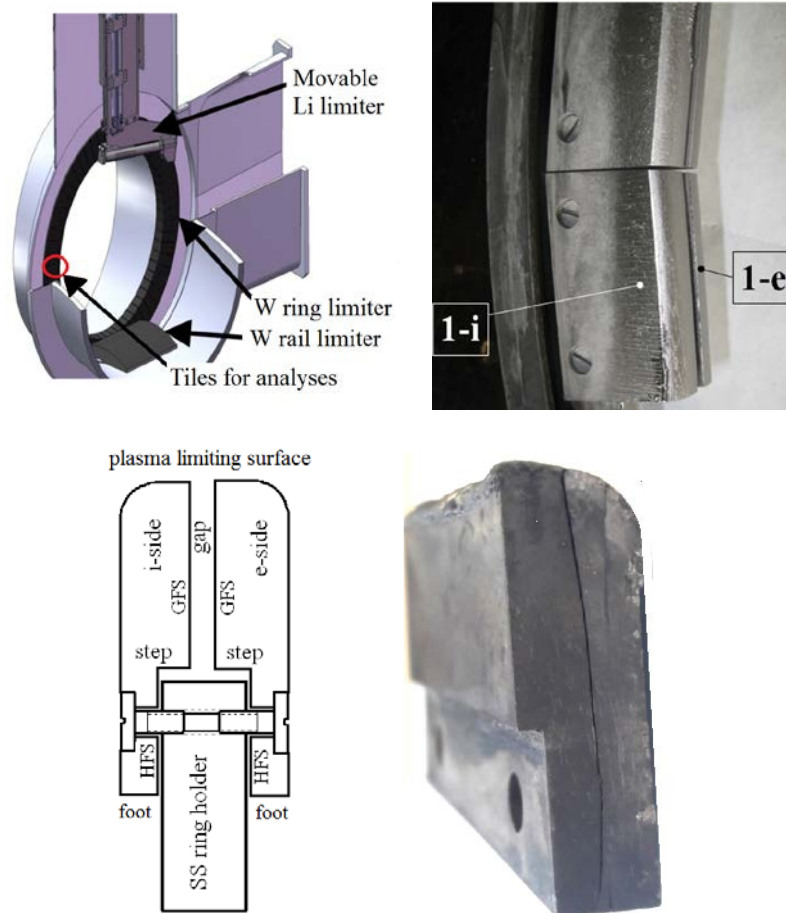

Figure 1. The arrangement of limiters in T-10, photo of tiles on the SS ring holder, the scheme of tiles on the holder, and photo of a damaged tile. Surfaces, which were investigated, are: gap facing surface GFS and holder facing surface HFS.

The W limiter was installed in 2015 and was used until decommissioning of T-10 in 2018. Before 2015, the limiter tiles were made of graphite MPG-8. For more than 40 years of operation of the tokamak, a significant part of the surface of the vacuum chamber was covered with thick "soft" and "hard" carbon films despite periodic cleaning discharges. Before replacing graphite tiles with tungsten tiles, the chamber walls were mechanically cleaned, though some carbon films could not

be removed. Besides the ring W limiter, there was a movable lithium limiter installed in the same toroidal section with the W limiter.

During the W limiter campaign from November 2015 to May 2018, about 4000 working pulses in deuterium and about 100 working pulses in helium with a duration of 1 s were made. About 400–500 shots were terminated by disruptions and the formation of the runaway electrons. In the stable discharges, as well as in the discharges with disruptions, plasma interacts most intensely with the outer and inner part of the ring limiter (near the equatorial plane) and the top of the rail limiter. Every night wall conditioning was performed in the inductive (Tailor) discharge in the longitudinal magnetic field. All in all 4000 h of cleaning discharges in deuterium and 50 h of discharges either in He or Ar (fifty-fifty) were performed. After every opening of the chamber, it was cleaned in the glow discharge (mainly in Ar and sometimes in He).

The tiles were subjected to various heat loads, which were maximal during disruptions. Tiles on the low-field side of T-10 experienced loads up to 1 GW/m^2, while the tiles on the high-field side were subjected to loads of 25-30 MW/m^2 maximum. The extra high thermal load of $1GW/m^2$ was connected with run-away electrons produced during disruptions (10^6 eV, 100 kA, 10 ms, 1 cm^2), which were created intentionally in 10% of the net number of discharges to test the tiles for extreme thermal loads. After decommissioning, the limiter was stored in air for a year before analyses. This paper presents the results of the study of two tiles 1i and 1e placed on the high-field side on the ion and electron sides, respectively. The attention was given to surfaces facing the gap between the tiles and surfaces facing the gap between the tiles and the ring holder.

Figure 2 and 3 demonstrate visual appearance of the shadowed surfaces of tile 1i (ion side) and tile 1e (electron side), respectively. The striking effect is that the surfaces in gaps, including the gap facing surfaces (GFS), SS holder facing surfaces (HFS), and the step between GFS and HFS are nonuniformly dark and violet and appear to be covered by a nonuniform film. This observation is in contrast with measurements of film deposition in castellated structures in TEXTOR [1, 22], where films thickness decreased towards the gap bottom with a fall-off length of about 1 mm.

Figures 2 and 3 demonstrate also droplets on the surfaces. The droplets on tile 1i are observed only close to the gap entrance at the plasma limiting surface (PLS), while droplets on tile 1e are observed very deep in the gap even near the step. Small droplets can be seen even in the very narrow gap between the tile and the SS holder.

Figure 2. Tile 1i as seen visually. General view, surface close to the entrance to the gap, and surface close to the step near the SS holder.

Figure 3. Tile 1e as seen visually. General view, surface close to the entrance to the gap, and surface close to the step near the SS holder.

3. Methods of analyses

For analyses of the surfaces of tiles, Laser Induced Breakdown Spectroscopy (LIBS), Scanning Electron Microscopy (SEM), Energy Dispersive Analyses (EDA), X-Ray Difraction (XRD), Thermal Desorption Spectroscopy (TDS), and Nuclear Reaction Analyses (NRA) were used.

LIBS analyses were performed using a homemade set-up based on a pulsed YAG: Nd^{3+} laser (Polus, Russia) with the wavelength of 1.064 μm and an optical spectrometer AvaSpec-2048. Optical spectrum emitted by atoms and ions of a plasma plume generated by a laser impulse is measured in this method. The LIBS set-up was not calibrated, therefore optical lines were used just to demonstrate presence of elements and did not give information about their concentrations. Scanning electron microscopy observations of tile surfaces and cross sections of tiles were performed using a microscope TESCAN VEGA 3 SBH. Energy dispersive analyses of concentrations of elements on the surface and on cross sections of tiles were performed using a spectrometer OXFORD INSTRUMENTS X-Max 2048. Phase analysis and measurements of stresses were made using a diffractometer BRUKER D8 Discover using $Cu-K_\alpha$ and $Cr-K_\alpha$ radiation. For interpretation of spectra, programs DIFFRAC.EVA, TOPAS, Leptos, LaboTex [28] and home-made programs [29] were used. Thermal desorption experiments were performed in a homemade UHV thermal desorption stand [30] equipped with a quadrupole mass spectrometer Hiden Hal 51 that permits to detect both D_2 and He using the method of threshold ionization mass spectrometry TIMS [31] by operation at different ionization energies. Nuclear reaction analysis of the deuterium depth profile was made on Tandem accelerator with 0.69 MeV, 1.2 MeV, 2.4 MeV, 3.2 MeV, and 4.5 MeV ^{3}He ions using nuclear reaction $D(^3He,p)^4He$ and the SIMNRA program [32] to analyze spectra.

4. Elemental composition of deposits.

Figure 4 demonstrates a result of LIBS analysis. Measurements were made in the central region of tile 1i at about 12 mm from the entrance to the gap. One can see that the spectrum contains lines of Li, C, O, N, Fe, Ni, W, Mo, He, and D. Lithium appears from the Li evaporator. Carbon appears from volatile hydrocarbons, which are emitted from the tokamak wall, as well as due to the contact of Li with air. The tungsten limiter never worked simultaneously with the graphite limiter, and the carbon deposited on the tiles may appear due to sputtering of carbon deposits on the wall, which were formed in previous campaigns with the graphite limiter. Tungsten is the material of the tile.

Iron, nickel, and chromium are elements of stainless steel wall and the ring holder. Molybdenum comes from the bolts attaching the W tiles to the SS ring. Oxygen and nitrogen appear due to chemical reactions of lithium with gases in air that may lead to formation of Li_2CO_3, Li_3N, and Li_2O. Deuterium was the working gas, and it was also used in cleaning discharges. Helium was used sometimes in cleaning discharges. LIBS measurements demonstrate that the wall, SS holder, limiters, gases used in discharges, and air gases contribute to deposits on the gap facing surface of the tile.
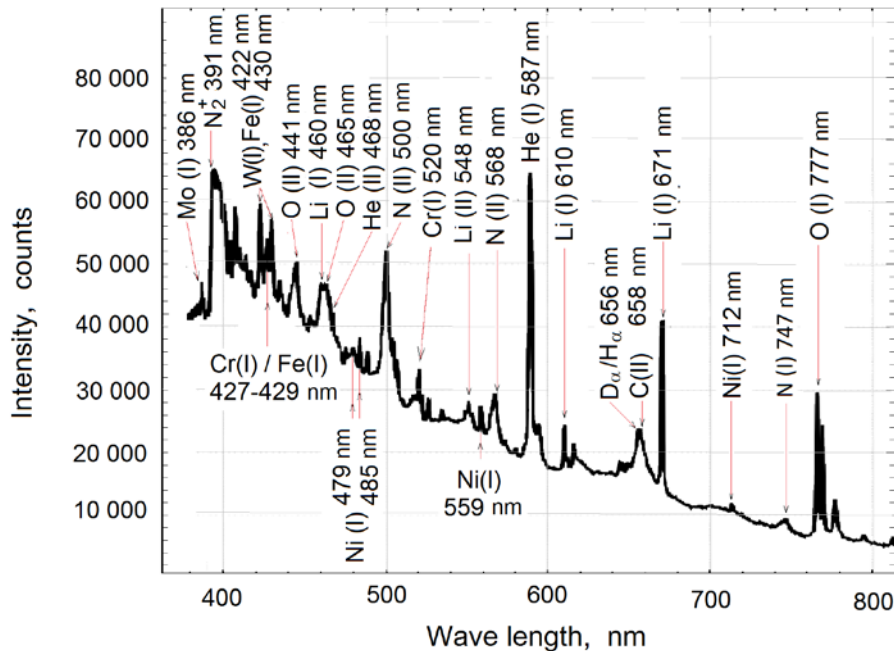

Figure 4. Optical spectra in LIBS measurements from tile 1i.

Analysis of the relative content of all elements, except for Li, D, and He, was made by SEM/EDA analyses. Figure 5 and Figure 6 demonstrate results of the analyses made on shadowed surfaces along the line from the bottom of the tile (x=0), which is far from the main plasma column, to the gap entrance, which is in contact with plasma (x=37mm). One can see that the main detected elements are carbon and oxygen. Tungsten signal is supposed to come from the substrate. One could suggest also that W might be co-deposited with Li. But the content of W in narrow gaps between the tile and the SS holder is more than 10at.%, and this seems to be too much for this suggestion, having in mind a high deposition rate of Li, low sputtering coefficient of W, and a small gap width of an order of 0.1 mm. Other materials are deposited in small quantities.

The ratio of O/C signals is about 3 for tile 1e. It was therefore suggested that the film on this tile is mainly composed of Li_2CO_3. Lithium can be vaporized from the Li limiter, which is placed over the gap between the tiles; besides Li droplets can appear at high heat loads on the Li limiter during abnormal events. One can see many droplets, with the O/C ratio close to 3, which were suggested to be Li_2CO_3 droplets. A large melted droplet with dimensions of about 5 mm was found even on the step of tile 1e 25 mm from the gap entrance. The Li droplets melted due to high temperature of tiles during discharges, and lithium wetted the entire surface of the tile as its wetting properties are very good [33]. Lithium penetrates even in the very narrow gap between the tile and the SS holder. Some droplets, which were deposited on late stages of tokamak operation, did not melt and remained on the surface. Besides Li droplets, a few number of small SS and Mo droplets were also observed.
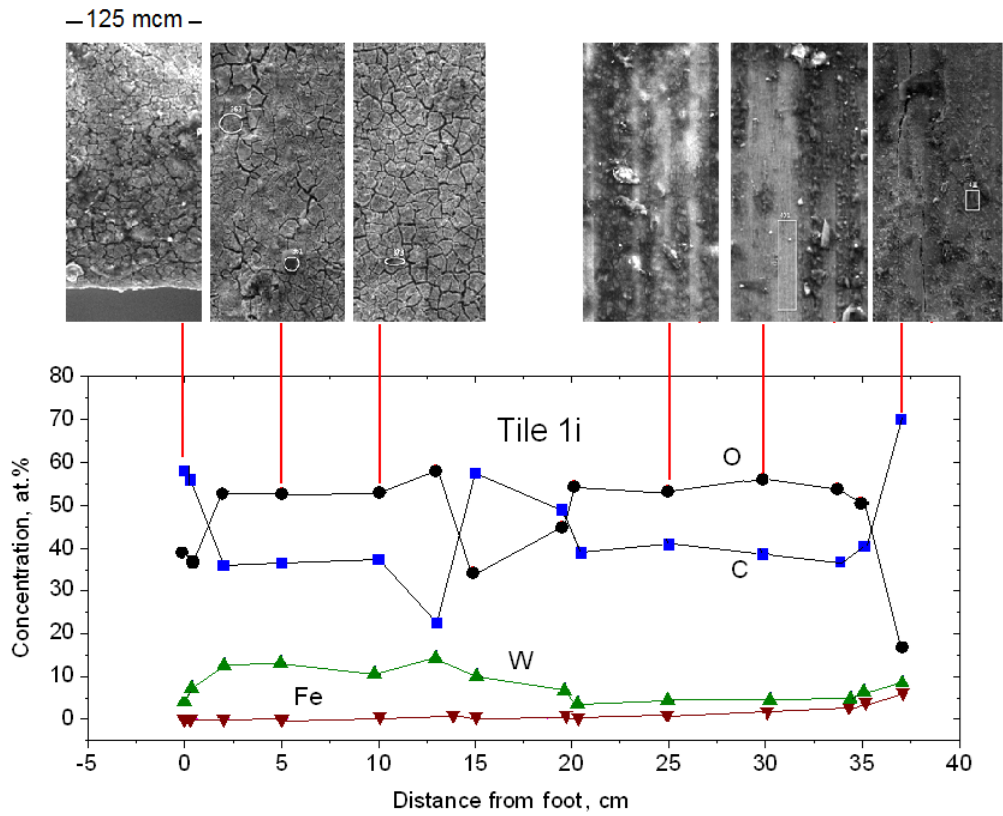
Figure 5. Concentration of elements on the shadowed side of tile 1i measured by SEM/EDA and SEM images of some areas, where concentrations were measured.
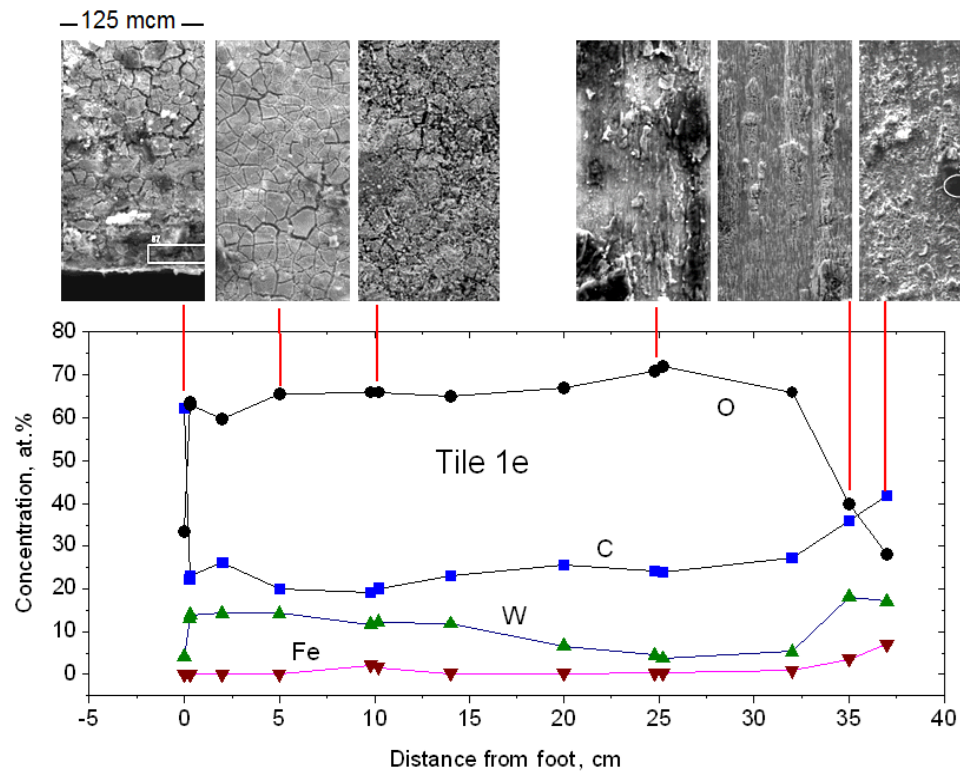

Figure 6. Concentration of elements on the shadowed side of tile 1e measured by SEM/EDA and SEM images of some areas, where concentrations were measured.

For tile 1i, the ratio of O/C is much less than 3. This means that the amount of carbon in the film exceeds that necessary to form Li carbonite, and this carbon was deposited during discharges. Carbon deposits were previously often observed in gaps between tokamak tiles, but those deposits were concentrated mainly within a few millimeters from the entrance to the gap [22]. The striking effect from figure 5 and 6 is that the concentration of carbon was approximately uniform on the tile in the interval x=2-32 mm from the bottom to the gap entrance. One must mention that the gap between the SS holder and the tile was very narrow (below 100 µm); nevertheless, large amount of carbon was deposited in this gap. This observation is in line with observations described in [24, 25], where carbon films were found in very narrow gaps between two surfaces tightly attached to each other. This was explained by decomposition of volatile hydrocarbons in the high frequency electric fields produced by auto-oscillating high frequency discharges in the magnetic field [24].

Oxygen in the film may appear mainly from air (either during air interventions in tokamak or after extraction of the tile from tokamak). It was demonstrated in [34] that Li films were about completely transformed to Li_2CO_3 after they had been exposed to air. Therefore, as the concentration of oxygen in the deposits on the tiles is more or less uniform over the surface at x in the range of 2-30 mm, one may conclude that the concentration of lithium is also more or less uniform in this range.

One must mention that figures 5 and 6 give just a qualitative distribution of the concentrations of elements measured by EDA, but not the amounts of the material deposited. This is because EDA cannot detect Li, and calculates the "concentrations" as if there is no Li in the film. Therefore increase and decrease of C and W depend on the thickness of the Li film on the surface, and decrease of O and increase of C and W near the edge in fig 5 and 6 are connected with decrease of Li near the edge due to its evaporation. The heat loads on tile 1e were higher than on tile 1i, and the Li (and O) depleted region became therefore wider. This is in line with observations that dark Li_2CO_3 films in figs 2 and 3 become light-colored closer to the entrance to the gap due to evaporation of Li. The foot of tiles is in shadow with respect to Li limiter, therefore the O signal in EDA spectra decreases there too.

5. Phase composition and stresses

X-Ray diffraction (XRD) spectrum taken from tile 1i in the middle area of the surface facing the gap is demonstrated in Figure 7. One can see peaks of W, WC, WO_2, Li_2CO_3, Li_2O, and Li_2WO_4. Tungsten carbides are formed presumably due to reaction of W with deposited C at high temperature. The final state of Li after long storage in air is Li_2CO_3. Therefore, presence of Li_2O and WO_2 may point to presence of oxygen in vacuum chamber due to either leak in the vacuum system or impurities in the gas supplied in the discharge.

XRD measurements were also used to determine stresses in the W tiles. Measurements were performed in the middle of tiles in two directions: parallel (X-direction) and perpendicular (Y-direction) to the long side of the tile. Measurements were performed using the standard $(\sin \psi)^2$ method. Namely, the shift of the diffraction angle Θ for plane (123) was measured as a function of the off-axis angle ψ, and the stresses were calculated using elastic constants for W. Compressive stresses were found in both directions for both tiles. The respective values were -458±22 and -118±15 MPa for tile 1i and -712±14 and -375±13 MPa for tile 1e. The compressive stresses in W can be explained by formation of carbides that have a larger unit cell volume compared with that in pure W.
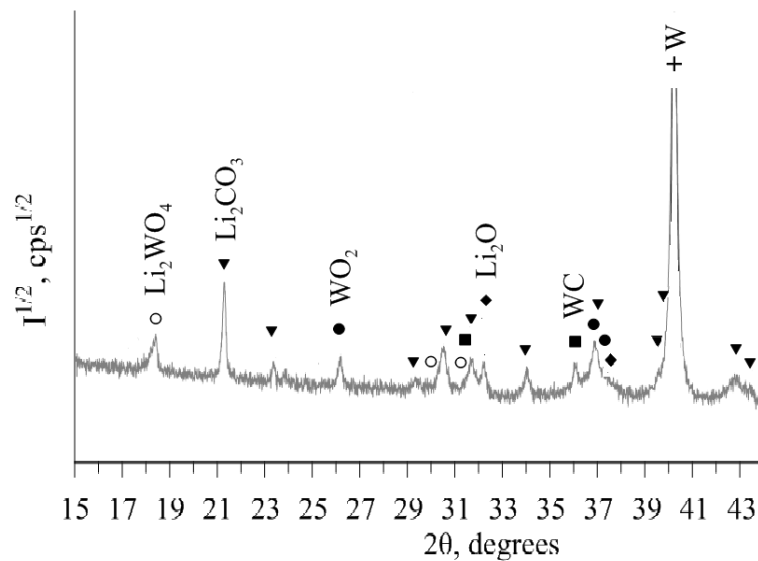
Figure 7. XRD spectrum taken from tile 1i on the gap facing surface.

Carbide phases were observed when analyzing cross-sections of the tiles using SEM/EDA. Figure 8 gives examples of SEM images of the cross-sections taken in back scattered electrons (BSE) together with carbon EDA maps given in red in three regions of tile 1e. The main elements in EDA maps of the cross sections are W and C. Other elements are on the level of noise. Carbon enriched regions interpreted as tungsten carbides, which were detected by XRD, are formed not only on surfaces facing the main gap, but also on surfaces facing the SS holder, where the gap between the tile and the SS holder is negligibly narrow. Carbide precipitates are often separated from the surface by a carbide-free layer of the order of 10 μm if to consider both SEM and EDA images. One may speculate that carbon deep under the surface may appear due to thermal diffusion, stress induced transport, and ion implantation.

Carbide precipitates often lead to appearance of cracks that propagate from the surface into the tile bulk. Also, plastic deformation of edges of tiles in plasma shadow was observed (figure 8), which was attributed to relaxation of stresses produced by carbides.

Non-uniformity of the surface transformation leads to strong difference of all mechanical properties of metal. As an example, the hardness measured in various areas of the gap facing and holder facing surfaces varied in a wide range from 500 $HV_{0.1}$, which is typical for tungsten, to 1200 $HV_{0.1}$, which is typical for tungsten carbides. Areas with enhanced hardness are brittle and demonstrate appearance of cracks.
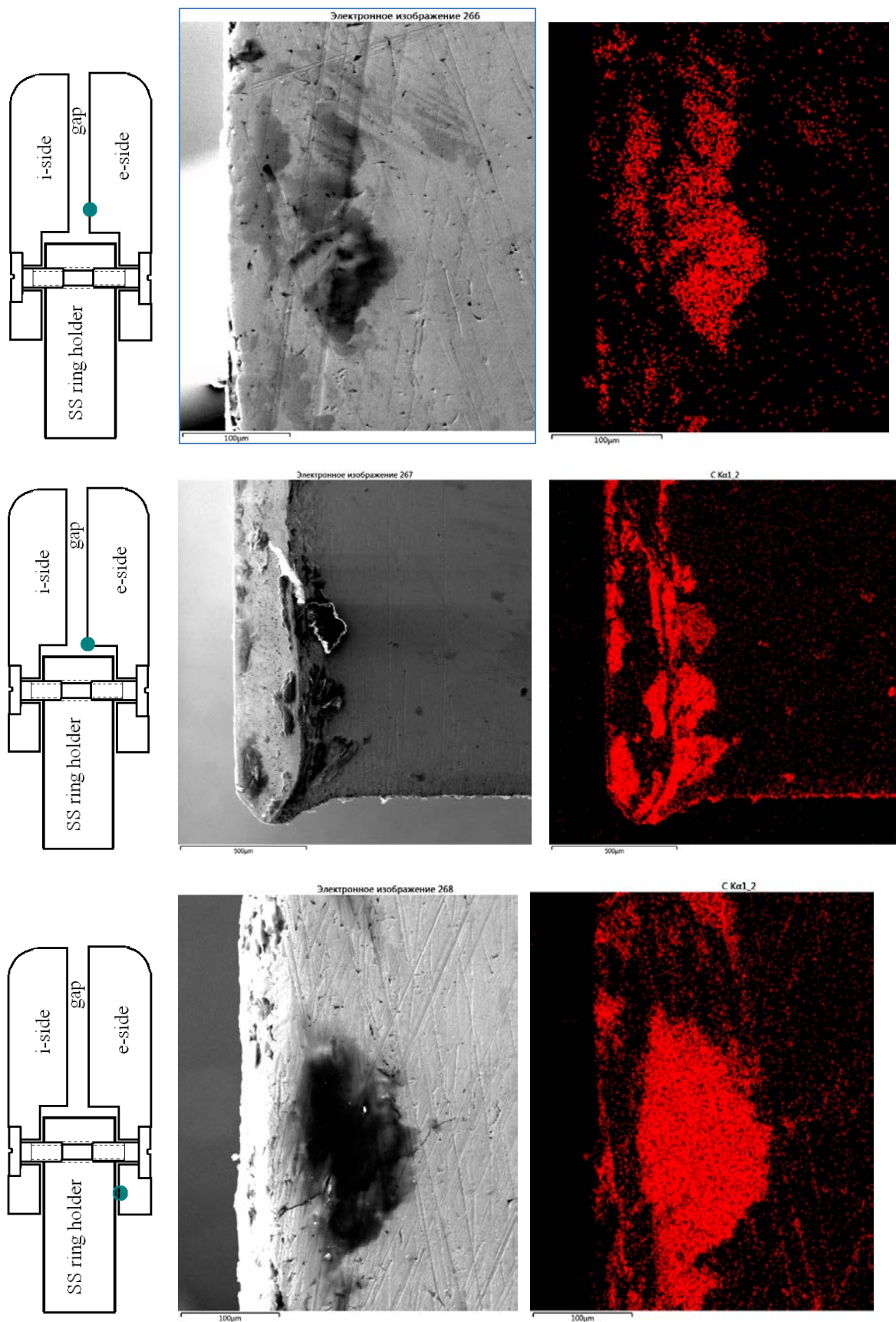
Figure 8. SEM/EDA observation of carbide precipitates on the cross sections of tile 1e in three regions marked by circles on the tile sketches on the left. The upper row is for the gap facing surface, the middle row is for the step between GFS and HFS, and the bottom row is for the holder facing surface. White & black images in the left column are BSE SEM images. Black & red images in the right column are EDA maps of the carbon concentration given by red color.

6. Deuterium and helium in tiles

Helium and deuterium trapping and release were measured by thermal desorption spectroscopy (TDS). Signals of D_2 and He (both m=4) were separated in the quadrupole mass spectrometer. Samples for TDS (8×8×1 mm) were cut from the gap facing side at several distances from the gap entrance.

It was shown in [39] that after the contact of co-deposited D-Li films with air, they completely transformed to Li_2CO_3, and no D remained in the resulting Li_2CO_3 films. Mechanical cutting of the samples was performed in water, and the Li_2CO_3 film was dissolved. After the lithium film was removed, a blackish carbon film was observed on the entire surface of the tile. This carbon film is suggested to appear in early lithium free campaigns of the tokamak operation due to decomposition of volatile hydrocarbons. Therefore one can expect that D and He, which are released during TDS measurements, are trapped not in the Li deposit, but in the W tile and in the deposited carbon film.

Figure 9 demonstrates TDS obtained for a sample cut from the gap facing side of tile 1e at a distance of about 1cm from the entrance to the gap. Desorption of D was observed in the temperature range of 600-1300 K, and desorption of He was at temperatures in the range of 1100-1700 K. The total amount of trapped D was of about $4×10^{17}$ D/cm^2. The number of trapped He was much less, about $7×10^{15}$ He/cm^2. Smaller amount of He with respect to D can be explained by smaller aggregate duration of discharges in helium with respect to discharges in deuterium. Deeper in the gap and close to the SS holder, the numbers of trapped D and He were about 2 orders of magnitude less than those close to the gap entrance. If accumulation of D in regions close to the SS holder could be explained both by deposition of volatile hydrocarbons and trapping of energetic particles (either ions or exited atoms) from plasma, trapping of the inert He can be explained only by implantation of energetic particles.

Recent analyses of desorption of ion implanted He from W [35] demonstrated that saturation level of trapped helium is of the order of 10^{17} He/cm^2 at various energies from 30 eV to 1 keV and temperatures from RT to 1200 K. Smaller amount observed in this work can be explained by a higher temperature of tiles.

Measurements of thermal desorption of He from C material IG-430 U implanted with 250-500 eV He ions [36] demonstrated that thermal desorption takes place in the ranges of 300−1100 K, 500−1100 K, and 700−1100 K if implantation was performed at 373K, 573 K, and 903 K, respectively. These temperatures are below the main range of He release in figure 9. Though low temperature peaks are observed in Fig. 9, their signal is at the level of the background. The main release is at higher temperatures. Contrary to release from carbon materials, experiments on helium ion implantation in W demonstrated high temperature TDS. In [35], release of He implanted in W at high temperatures was observed in a range of 1600-2500 K. In another work [37], W was subjected to He glow discharge, and TDS was observed at temperatures in the range of 1000-1600 K, that correlates with the range of He release in figure 9. One may therefore suggest that He release is not from carbon deposits, but mainly from W, where it appears due to ion implantation during cleaning in He discharges.

Experimental measurements of deuterium TDS from W after low flux D ion implantation demonstrated D_2 release with peaks from 400 K to 600 K [38-40], which disagree with results given in figure 9. Contrary, experiments [41] with W and with W doped with Ti carbides demonstrated peaks at 800 K and 1000 K that perfectly correlates with peaks in figure 9. That is, deuterium may also appear in the tiles due to ion implantation from the regular and cleaning discharges in deuterium. Carbide precipitates are suggested to play an important role in D retention.
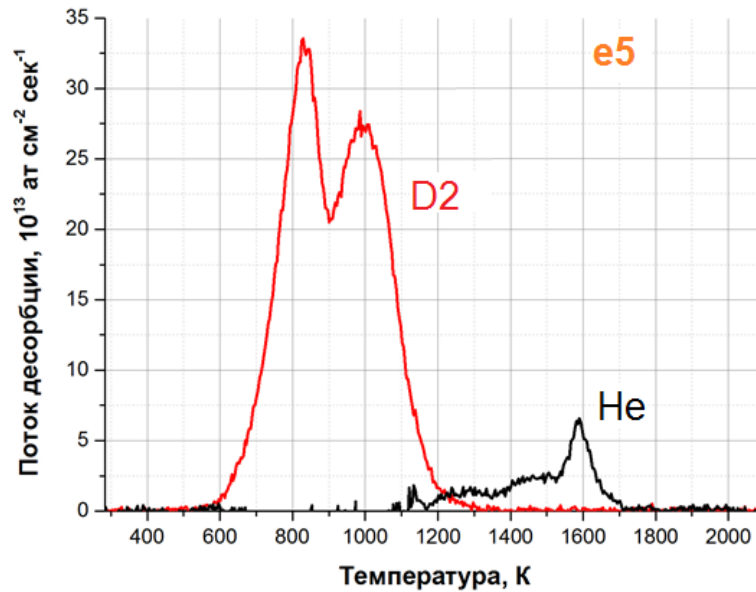
Figure 9 TDS obtained for a sample cut from the gap facing side of tile 1e close to the entrance to the gap. The rate is 2 K/s.

At the same time, deuterium may appear also due to decomposition of hydrocarbons. Indeed, thermal desorption measurements [42] of D release from "hard" C films deposited on T-10 walls demonstrated a peak at 850 K and a wide desorption region 900-1400 K in agreement with the temperature range in figure 9. Carbon deposits observed on the tile surface are black in color, and this is typical for hard films with a low concentration of hydrogen. Deuterium trapping in carbon based materials give a very wide range of release temperatures depending on the material and ways of D introduction [42, 43]. Nevertheless, the temperature of the tiles rose above the temperature sufficient for deuterium release from the film, so the accumulation is supposed to take place mainly in tungsten.

Figure 10 demonstrates the deuterium profile measured by NRA at a distance of 4-10 mm from the gap entrance. One can see that deuterium penetrates to depths of several μm. The total number of trapped deuterium trapped within 7 μm is 2×10^{16} D/cm^2. This value is much less, than that obtained by TDS in samples positioned at the same distance from the gap entrance. One may suggest therefore that D is trapped not only near the surface, but also rather deep in the bulk at distances not available for NRA. This trapping can be explained by D diffusion and trapping in defects in the bulk. The deuterium profile is peaked at a distance from the surface, and this can point to the ion implantation in tungsten. So, TDS and NRA measurement can be explained by deuterium trapping both in carbon deposits and in the W tiles, though accumulation in carbon films seems unlikely, while ion trapping in W seems preferential.
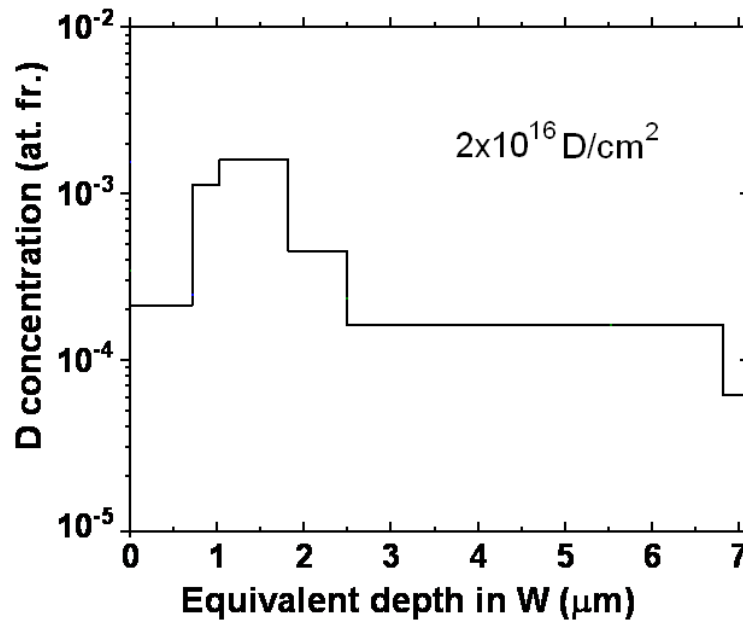
Figure 10. Deuterium profile in tile 1i measured in the middle area of the tile by NRA.

7. Discussion

Carbon in tokamaks can be deposited both during regular and conditioning discharges. In T-10, conditioning discharges led to deposition of soft (hydrogen reach) films, while regular discharges – to deposition of hard (hydrogen depleted) films. Soft films on probes in T-10 were never observed if the temperature exceeded 220°C either during or after deposition. The temperature of tiles, which we investigated, was much higher, therefore the films on the tiles were hard films deposited during regular discharges but not during the conditioning discharges. Hard films are stable at high temperatures contrary to deuterium reach soft films.

The entire gap facing surface, after the lithium film had been washed out, was covered by a black carbon film, and this color is typical for hard films. The peculiar effect was that surfaces of tiles, which were attached to the SS holder with a very narrow gap (below 0.1 mm) between them, were also covered by a carbon film. Neither regular no conditioning discharges can penetrate this narrow gap. Films in the narrow gap were very similar to those deposited in the wide gap between the two tiles facing each other. One may suggest that films in the narrow gaps, as well as those in wide gaps, were deposited in regular discharges.

One can hardly expect that particles from plasma may penetrate so deep into so narrow gaps. For explanation of this observation, we suggest a mechanism associated with auto-oscillating discharges, which was proposed in [24-26]. These discharges arise between two surfaces (for example the external surface of a W tile and the wall of the tokamak) connected by the magnetic field. The condition for the discharge is a high secondary electron-electron emission from one of the surfaces. Enhanced electron emission is typical for thin dielectric films on the surface, and the auto-oscillating discharges were observed on W with a thin oxide film on the surface [26]. Tungsten oxides on T-10 limiters were found in [27] and in this work. If the contact of plasma with this surface has an N-shaped current-voltage characteristic, it acts as an amplifying element with positive feedback, which can lead to instabilities of the current in the circuit consisting of plasma and two surfaces, connected by conductive structural elements of the tokamak chamber. These

instabilities excite high frequency self-oscillations of various types, as well as secondary unipolar discharges through plasma. Both plasma, sheath, and other parts of the circuit have their own capacitances and inductivities that determine the parameters of these oscillations. The energy source for the discharge is the plasma filament connecting both surfaces.

In the case of the two W tiles in T-10, unipolar auto-oscillating discharges can appear on external surfaces of both tiles independently. The current through plasma between a tile and another surface in tokamak (the wall for example) is closed by structural elements (vacuum wall, ring holder, etc.). The tile itself is also a part of the circuit; so the high frequency current passes through the tile to the SS ring holder. This current provokes high frequency electric fields in the gap, and these fields are supposed to be the reason of dissociation of volatile hydrocarbons and C deposition on surfaces in the gap. The effect was demonstrated in [24, 25], where preferential deposition of carbon films in very narrow gaps (below 0.1 mm) was associated with high frequency electric fields produced by high frequency currents through the gap facing surfaces. Frequencies were estimated to be of about 50 MHz, and the electric field strength was estimated to be 10^7 V/m in [24] and 1.5×10^4 V/m in [25].

High electric fields in the gap can also ionize C, D, and He atoms and accelerate the ions, so that their accumulation can be partly explained by ion implantation. TDS of deuterium has features of both D-C co-deposition and D ion implantation; and NRA of deuterium and TDS of He can be explained by ion implantation. Besides, formation of carbides far from the surface may be explained by carbon ion implantation.

8. Conclusions

Surfaces of two W tiles facing gaps in the T-10 ring limiter were analyzed using SEM/EDS, LIBS, XRD, TDS, and NRA methods. All surfaces were completely covered by deposits, which contained C, O, N, Li, D, He, Fe, Ni, and Mo. Droplets of Li, SS, and Mo were observed. Lithium in gaps appeared from Li limiter due to evaporation and splashing of its surface with subsequent deposition on tiles and wetting their entire surfaces at high temperatures including the surfaces facing the very narrow gap between the tile and the SS holder. The deposited Li was transformed to Li_2CO_3 after contact with air. Some Li was found in the oxide state. Oxygen and carbon in the film were due to chemical reactions with lithium in air. Carbon was suggested also to appear due to deposition and dissociation of volatile hydrocarbons in plasma discharges. Mainly regular but not cleaning discharges were suggested to lead to carbon deposition. Carbon was found on the entire surface of the very narrow gaps (0.1 mm) between the W tiles and the SS holder. The explanation of this finding was relied on the effect of high frequency auto-oscillating discharges, which can appear on the plasma-facing surfaces of the tiles, and induce strong high frequency electric fields in the gap. These fields lead to decomposition of volatile hydrocarbons and ionization of carbon; so that carbon can be both deposited on the surface and implanted in W.

Accumulation of deuterium and helium is presumably associated with implantation of ions produced in the high frequency and high voltage electric fields that appear in gaps due to auto-oscillating discharges. Carbide precipitates make available variety of trapping sites for D and He trapping. Deuterium may also be trapped in "hard" carbon films deposited on the surface.

Phase precipitates of WC, WO_2, Li_2CO_3, Li_2O, and Li_2WO_4 were detected close to the surface. Massive tungsten carbides at depths up to 1 mm were observed over the entire surface including the surfaces in the very narrow gaps. Carbide formation provoked cracks propagation into the bulk.

Compressive stresses were measured in tungsten. The mechanical properties over the surfaces of two tiles were very non-uniform.

Acknowledgements

References

[1] A. Kreter, P. Wienhold, H.G. Esser, A. Litnovsky, V. Philipps, K. Sugiyama, TEXTOR Team, Long-term carbon transport and fuel retention in gaps of the main toroidal limiter in TEXTOR, Journal of Nuclear Materials 438 (2013) S746-S749.

[2] J.W. Davis, C.K. Tsui, G.A. Chung, B.W.N. Fitzpatrick, A.A. Haasz, Thermo-oxidation of DIII-D codeposits on open surfaces and in simulated tile gaps, Journal of Nuclear Materials 415 (2011) S789-S792.

[3] A. Kreter, S. Brezinsek, J.P. Coad, H.G. Esser, W.Fundamenski, V. Philipps, R.A. Pitts, V. Rohde, T. Tanabe, A. Widdowson, JET EFDA contributors, Dynamics of erosion and deposition in tokamaks, Journal of Nuclear Materials 390–391 (2009) 38-43.

[4] T. Loarer, Fuel retention in tokamaks, Journal of Nuclear Materials 390–391 (2009) 20-28.

[5] I. Tanarro, J.A. Ferreira, V.J. Herrero, F.L. Tabarés, C. Gómez-Aleixandre, Removal of carbon films by oxidation in narrow gaps: Thermo-oxidation and plasma-assisted studies, Journal of Nuclear Materials 390–391 (2009) 696-700.

[6] F. Ghezzi, A. Tolstogouzov, Boron deposition on the graphite tiles of the RFX device studied by secondary ion mass spectrometry, Journal of Nuclear Materials 373 (2008) 402-406.

[7] T. Tanabe, K. Sugiyama, T. Renvall, J. Likonen, L. Penttinen, E. Vainonen-Ahlgren, J.P. Coad, Tritium distribution measurement of JET Mk II SRP divertor tiles, Journal of Nuclear Materials 363–365 (2007) 960-965.

[8] M. Yoshida, T. Tanabe, A. Adachi, T. Hayashi, T. Nakano, M. Fukumoto, J. Yagyu, Y. Miyo, K. Masaki, K. Itami, Carbon transport and fuel retention in JT-60U with high temperature operation based on postmortem analysis, Journal of Nuclear Materials 438 (2013) S1261-S1265.

[9] R.D. Penzhorn, N. Bekris, W. Hellriegel, H.E. Noppel, W. Nägele, H.Ziegler, R. Rolli, H. Werle, A. Haigh, A. Peacock, Tritium profiles in tiles from the first wall of fusion machines and techniques for their detritiation, Journal of Nuclear Materials 279 (2000) 139-152.

[10] M.J. Rubel, J.P. Coad, D. Hole, JET-EFDA Contributors1, Overview of long-term fuel inventory and co-deposition in castellated beryllium limiters at JET, Journal of Nuclear Materials 386–388 (2009) 729-732.

[11] Suk-Ho Hong, Sang-Joon Park, Jae-Myung Choe, Young-Mu Jeon, Seung Jae Yang, Sun-Taek Lim, Sooseok Choi, Young-Gil Jin, Chong Rae Park, Gon-Ho Kim, Deposition/erosion and H/D retention characteristics in gaps of PFCs in KSTAR studied by cavity technique, Journal of Nuclear Materials 438 (2013) S698-S706.

[12] J.P. Coad, M. Rubel, C.H. Wu, The amount and distribution of deuterium retained in the JET divertor after the C and Be phases in 1994–1995, Journal of Nuclear Materials 241–243 (1997) 408-413.

[13] H. Roche, Ph. Delaporte, C. Grisolia, P. Languille, T. Loarer, C. Martin, S. Panayotis, J.-Y. Pascal, B. Pégourié, E. Tsitrone, Layer removal in gaps by laser process, Journal of Nuclear Materials 438 (2013) 1079-S1083.

[14] M. Mayer, V. Philipps, P. Wienhold, H.G. Esser, Jvon Seggern, M. Rubel, Hydrogen inventories in nuclear fusion devices, Journal of Nuclear Materials 290–293 (2001) 381-388.

[15] C. Brosset, H. Khodja, Tore Supra team, Deuterium concentration in deposited carbon layers in Tore Supra, Journal of Nuclear Materials 337–339 (2005) 664-668.

[16] D. Matveev, A. Kirschner, H.G. Esser, M. Freisinger, A. Kreter, O. Van Hoey, D. Borodin, A. Litnovsky, P. Wienhold, J.W. Coenen, H. Stoschus, V. Philipps, S. Brezinsek, G. Van Oost, the TEXTOR team, Carbon deposition at the bottom of gaps in TEXTOR experiments, Journal of Nuclear Materials 438 (2013) S775-S779.

[17] H.S. Barnard, B. Lipschultz, D.G. Whyte, A study of tungsten migration in the Alcator C-Mod divertor, Journal of Nuclear Materials 415 (2011) S301-S304.

[18] Wolfgang Jacob, Redeposition of hydrocarbon layers in fusion devices, Journal of Nuclear Materials 337–339 (2005) 839-846.

[19] J. Roth, E. Tsitrone, A. Loarte, Th. Loarer, G. Counsell, R. Neu, V. Philipps, S. Brezinsek, M. Lehnen, P. Coad, Ch. Grisolia, K. Schmid, K. Krieger, A. Kallenbach, B. Lipschultz, R. Doerner, R. Causey, V. Alimov, …A. Kukushkin, Recent analysis of key plasma wall interactions issues for ITER, Journal of Nuclear Materials 390–391 (2009) 1-9.

[20] H. Bergsåker, I. Bykov, P. Petersson, G. Possnert, J. Likonen, S. Koivuranta, J.P. Coad, A.M. Widdowson, JET EFDA contributors, Microstructure and inhomogeneous fuel trapping at divertor surfaces in the JET tokamak, Nuclear Instruments and Methods in Physics Research Section B: Beam Interactions with Materials and Atoms 332 (2014) 266-270.

[21] S. Krat, Yu. Gasparyan, A. Pisarev, M. Mayer, JET-EFDA contributors, Hydrocarbon film deposition inside cavity samples in remote areas of the JET divertor during the 1999–2001 and 2005–2009 campaigns, Journal of Nuclear Materials 463 (2015) 822-826.

[22] A. Litnovsky, V. Philipps, A. Kirschner, P. Wienhold, G. Sergienko,A. Kreter, U. Samm, O. Schmitz, K. Krieger, P. Karduck, M. Blome, B. Emmoth, M. Rubel, U. Breuer, A. Schol, Carbon transport, deposition and fuel accumulation in castellated structures exposed in TEXTOR, Journal of Nuclear Materials 367–370 (2007) 1481–1486.

[23] A. Litnovsky, V. Philipps, P. Wienhold, A. Kreter, et al., Material migration and mixing, fuel retention and cleaning of ITER-like castellated structures in TEXTOR, Journal of Nuclear Materials 415 (2011) S289–S292

[24] I.V. Vizgalov, A.A. Pisarev, K.M. Gutorov, A mechanism of PFM erosion and redeposition in gaps, Journal of Nuclear Materials 363–365 (2007) 966-971.

[25] K. Gutorov, I. Vizgalov, F. Podolyako, I. Sorokin, Film deposition and their removal in gaps and regions shaded from the plasma in the presence of RF fields, Physics Procedia 71 (2015) 68 – 72

[26] K. M. Gutorov, I. V. Vizgalov, I. A. Sorokin, and F. S. Podolyako, Current–Voltage Characteristic of the Contact of a Plasma with an Electrode with a Thin Dielectric Film on the Surface, JETP Letters 100 (2014) 708–711.

[27] S.A. Grashin, I.I. Arkhipov, V.P. Budaev, A.V. Karpov, L.A. Klyuchnikov, L.N. Khimchenko, A.V. Melnikov, D.V. Sarychev, N.S. Sergeev, I.A. Zemtsov, ITER-grade tungsten limiters damage under high turbulent heat flux in the T-10 tokamak, Fusion Engineering and Design 146 (2019) 2100–2104

[28]. K. Pawlik Determination of the orientation distribution function from pole figures in arbitrarily defined cells, Phys. Stat. Sol. (b). (1986) p. 477.

[29]. M. Isaenkova,Yu. Perlovich, V. Fesenko, Modern methods of experimental construction of texture complete direct pole figures by using X-ray data, IOP Conf. Series: Materials Science and Engineering 130 (2016) 012055.

[30] A. Rusinov, Yu. Gasparyan, S. Perelygin, A. Pisarev, S. Stepanov, N. Trifonov, A setup for thermodesorption measurements, Instrum. Exp. Tech. 52 (2009) 871–876.

[31] S. Davies, J.A. Rees, D.L. Seymour, Threshold ionization mass spectrometry (TIMS); a complementary quantitative technique to conventional mass resolved mass spectrometry, Vacuum 101 (2014) 416-422.

[32] M. Mayer, SIMNRA User's Guide, Report IPP 9/113, Max-Planck-Institut für Plasmaphysik, Garching, Germany, 1997.

[33] S.A. Krat, A.S. Popkov, Yu. M. Gasparyan, A.A. Pisarev, Peter Fiflis, Matthew Szott, Michael Christenson, Kishor Kalathiparambil, David N. Ruzic, Wetting properties of liquid lithium on lithium compounds, Fusion Engineering and Design 117 (2017) 199–203.

[34] Yu. M. Gasparyan, A.S. Popkov, S.A. Krat, A.A. Pisarev, Ya.A. Vasina, I.E. Lyublinski, A.V. Vertkov, Deuterium release from Li-D films exposed to atmospheric gases, Fusion Engineering and Design 117 (2017)163–167

[35] S. Ryabtsev, Yu. Gasparyan, V. Efimov, Z. Harutyunyan, A. Aksenova, A. Poskakalov, A. Pisarev, S. Kanashenko, Yu. Ivanov, Helium retention in tungsten irradiated with He+ ion beam at elevated temperatures, Nuclear Instruments and Methods in Physics Research Section B: Beam Interactions with Materials and Atoms 460 (2019) 108-113.

[36] M. Oya, G. Motojima, M. Tokitani, H. Tanaka, Y. Ueda, The role of the graphite divertor tiles in helium retention on the LHD wall, Nuclear Materials and Energy13 (2017) 58-62.

[37] Y. Kubota, N. Noda, A. Sagara, H. Suzuki, S. Masuzaki, K. Tokunaga, T. Satow, K. Yamazaki, O. Motojima, Investigation of the trapped helium and hydrogen ions in plasma facing materials for LHD using thermal desorption spectrometer and alternating glow discharge cleanings, Journal of Nuclear Materials 313–316 (2003) 239–244.

[38] M. Zibrov, S. Ryabtsev, Yu. Gasparyan, A. Pisarev, Experimental determination of the deuterium binding energy with vacancies in tungsten, Journal of Nuclear Materials 477 (2016) 292-297.

[39] A.A. Pisarev, A.V. Varava, S.K. Zhdanov, Ion implantation of deuterium in tungsten, Journal of Nuclear Materials 220–222 (1995) 926-929.

[40] A. Rusinov, Yu. Gasparyan, N. Trifonov, A. Pisarev, S. Lindig, M. Sakamoto, Investigation of hydrogen-defect interaction in tungsten by the probe fluence method, Journal of Nuclear Materials 415 (2011) S645-S648.

[41] M. Zibrov, M. Mayer, L. Gao, S. Elgeti, H. Kurishita, Yu. Gasparyan, A. Pisarev, Deuterium retention in TiC and TaC doped tungsten at high temperatures, Journal of Nuclear Materials 463 (2015) 1045-1048.

[42] A. Pisarev, Yu. Gasparyan, A. Rusinov, N. Trifonov, V. Kurnaev, A. Spitsyn, B. Khripunov, T. Schwarz-Selinger, M. Rasinski, K. Sugiyama, Deuterium thermal desorption from carbon based materials: A comparison of plasma exposure, ion implantation, gas loading, and C–D codeposition, Journal of Nuclear Materials 415 (2011) S785-S788.

[43] A. Pisarev, T. Tanabe, B. Emmoth, N. Trifonov, B. Khripunov, Deuterium accumulation in carbon materials at high fluence, Journal of Nuclear Materials 390–391 (2009) 677-680.